GEOPHYSICAL RESEARCH LETTERS, VOL. 27, NO. 19, PAGES 3101-3104, OCTOBER 1, 2000

Near real-time radar interferometry of the Mw 7.1 Hector Mine Earthquake

David T. Sandwell, Lydie Sichoix, Duncan Agnew, Yehuda Bock and Jean-Bernard Minster
Scripps Institution of Oceanography, La Jolla, California

Abstract. The Hector Mine Earthquake (Mw 7.1, 16 October 1999) ruptured 45 km of previously mapped and unmapped faults in the Mojave Desert. The ERS-2 satellite imaged the Mojave Desert on 15 September and again on 20 October, just 4 days after the earthquake. Using a newly-developed ground station we acquired both passes and were able to form an interferogram within 20 hours of the second overflight. Estimates of slip along the main rupture are 1-2 meters greater than slip derived from geological mapping. The gradient of the interferometric phase reveals an interesting pattern of triggered slip on adjacent faults as well as a 30 mm deep sink hole along Interstate 40.

Introduction

The eastern California shear zone (ECSZ) accommodates a significant portion of strike-slip motion ($\sim$ 12 mm/yr) between the Pacific and North American plates [*Dokka and Travis*, 1990; *Sauber et al.*, 1994]. During the past 10 Ma, strain in the ECSZ has shifted westward so that today, the Ludlow Fault (LD in Figure 1) is believed to be the easternmost active fault in the region. The recent Hector Mine earthquake ruptured 45 km along the mapped, but unnamed, Lavic Lake fault [*Dibblee*, 1966; *USGS et al.*, 2000] just 7.3 years after the Landers Mw 7.3 event. These two major events may have increased the loading on the San Andreas [*Stein et al.*, 1992].

Near real-time interferometry

We report on the use of synthetic aperture radar interferometry (InSAR) to map crustal strain in near real-time. While the InSAR method is well developed [*Massonnet et al.*, 1993; *Zebker et al.*, 1994; *Peltzer et al.*, 1996; *Rosen et al.*, 1996; *Massonnet and Feigl*, 1998], results have always been published months or even years after events. For example, many small-scale fractures associated with the Landers, 1992 event were not noticed in ERS interferograms until 2-4 years after the rupture, by which time evidence of the displacements had been erased by natural forces and off-road vehicles [*Massonnet et al.*, 1994; *Price and Sandwell*, 1998].

InSAR processing software, ground-station capabilities, and real-time orbits [*Scharroo and Visser*, 1998] have improved to the point where near real-time interferometry is possible. The Hector Mine earthquake offered the first meaningful test of our X-band receiving station and interferometry software (topex.ucsd.edu). To prepare for the 20 October pass, we assembled prior ERS passes over the area. Fourteen frames were available including an ERS-1/ERS -2 tandem pair having a 1-day time separation and a 95 m perpendicular baseline (E1_24664 and E2_04991). This pair was unwrapped using the tree algorithm [*Goldstein et al.*, 1988] to serve as the topographic phase for the, still to be determined, deformation pair. Beginning in June 1999 we began ordering all overflights along this trackline from SpotImage Co. so our local archive contained passes from June, July, August, and September. One day prior to the overflight we obtained the predicted ERS-2 orbit from Delft University [*Scharroo and Visser*, 1998] and established that the best interferometric match was the 15 September pass. Fortunately, in an effort to re-image the area devastated by the Izmit Turkey earthquake, ESA navigated the 20 October pass to within 17 m perpendicular baseline of the 15 September pass; a typical 1-month baseline is about 500 m.

During interferogram formation, the phase due to both the curvature of the earth and the topography was removed from the full resolution interferogram on a pixel-by-pixel basis using precise orbital information [*Scharroo and Visser*, 1998]. The first interferogram, formed 19 hours after the download, had an artificial cross-track slope of 20 fringes (560 mm) caused by errors in the predicted orbit. The interferogram was re-computed 5 days later using the more accurate "fast-delivery" orbit and no slope corrections were needed (Figure 2). Indeed, given precise orbits and precise topography, we believe that it is unnecessary to flatten interferograms. Moreover, flattening may mask the desired tectonic signal.

The coherence of the interferogram was generally very high because of the short time interval of the reference and repeat passes, the short interferometric baseline, and the arid, unvegetated surface of the Mojave Desert. The high coherence permitted phase unwrapping almost everywhere except the areas close to the main rupture where the phase rate exceeded one half cycle per pixel or the ground displacement approached the azimuthal resolution of the SAR image [*Michel and Avouac*, 1999]. In addition to computing phase, we computed the phase gradient following the approach of Price and Sandwell [1998]. Both the unwrapped phase and the phase gradient are needed to interpret the complex displacement patterns in the area surrounding the main rupture. Phase gradient maps were provided to field geologists within a week after the earthquake to aid their mapping efforts. One of the more interesting features of the interferogram is a 30 mm deep, 1 km diameter sinkhole on the southern margin of Troy Dry Lake bed (34.805, -116.525); Interstate-40 passes directly over this sinkhole.

Displacement along the main rupture

Because of the large ground displacements, the main rupture is partly decorrelated in the interferogram. However,

Copyright 2000 by the American Geophysical Union.

Paper number 1999GL011209.
0094-8276/00/1999GL011209$05.00

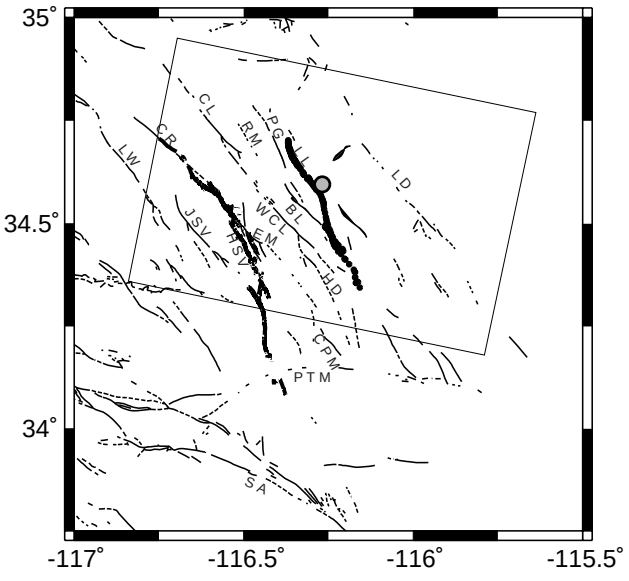

Figure 1. Location of the descending ERS SAR frame containing the Hector Mine Earthquake. Fault abbreviations: Lenwood (LW), Johnson Valley (JSV), Homestead Valley (HSV), Emerson (EM), Copper Mountain (CPM), Camp Rock (CR), Calico (CL), West Calico (WCL), Rodman (RM), Pisgah (PG), Bullion Mountain (BL), Hidalgo (HD), Lavic Lake (LL), Ludlow (LD), Pinto Mountain (PTM), and San Andreas (SA).

by counting fringes one can still estimate the line-of-sight (LOS) ground displacement across the fault Figure 2, inset). The trace of the Lavic Lake fault was recently mapped by a

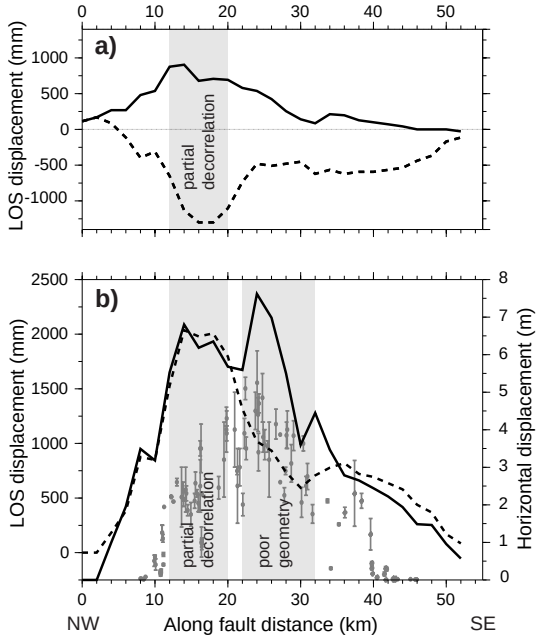

Figure 3. a) Line-of-sight (LOS) displacement along the surface rupture from north to south in 2 km increments estimated by counting interferometric fringes, dashed-east, solid-west. **b)** total LOS displacement (dashed, left scale) reaches a maximum of 2.0 m at 16 km from the north end of the fault. Assuming pure strike-slip displacement (solid, right scale), the maximum horizontal displacement is > 7 m at a distance of 24 km. Field estimates of slip (grey points and uncertainties) are 1-2 meters lower than InSAR estimates.

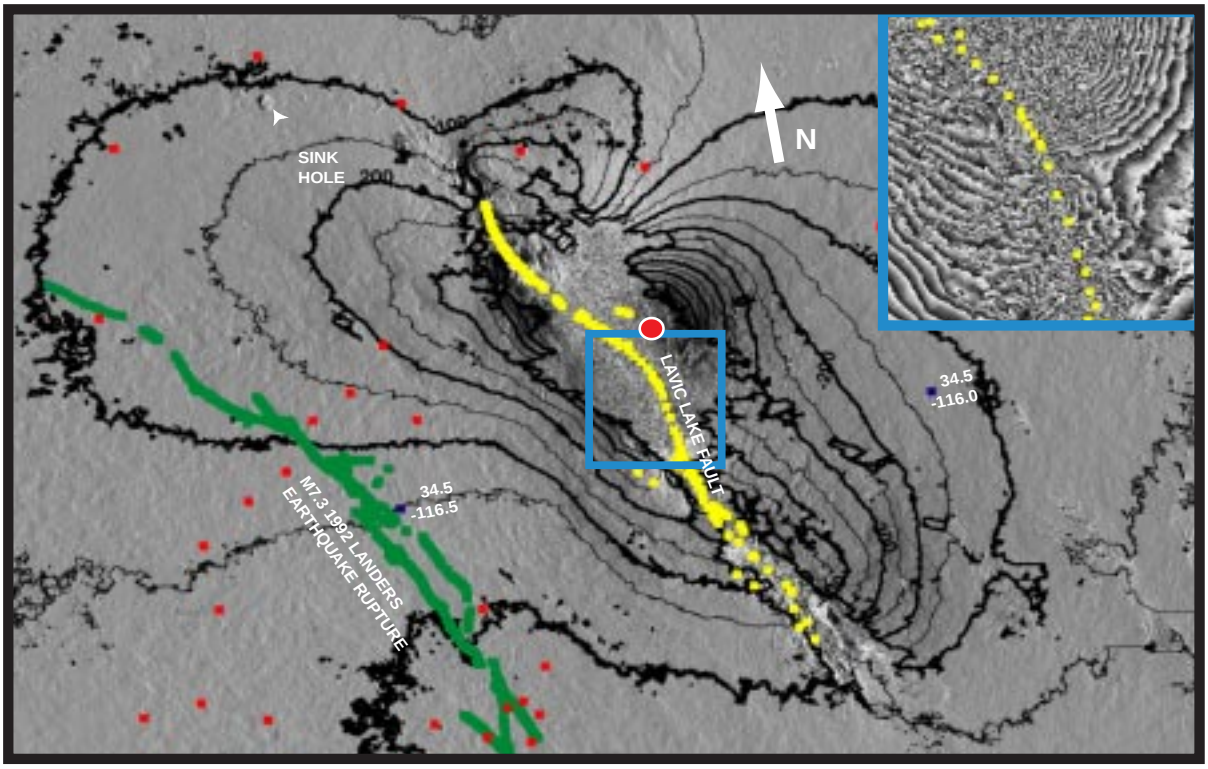

Figure 2. Contours of line-of-sight displacement (mm) of the ground away from the radar. Grey-scale represents the east component of the phase gradient; note the sink hole at 34.805, -116.525. Red circle is epicenter, yellow squares are the surface rupture, green line is Landers 1992 surface rupture, red dots are locations of GPS monuments surveyed prior to the Hector Mine earthquake. The phase nearby the fault could not be unwrapped however, the fringes were clear enough to count (inset, upper right).

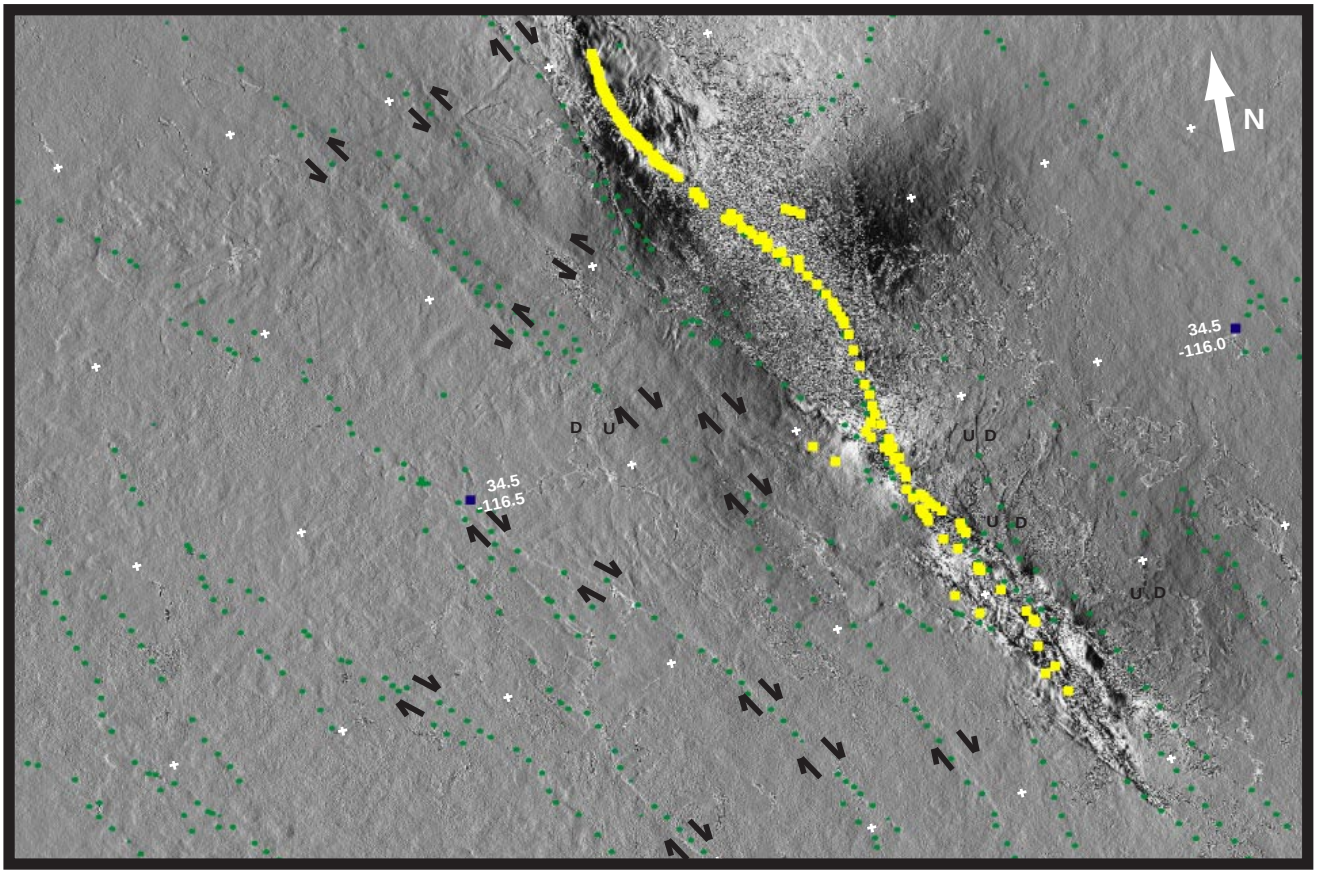

Figure 4. Lineaments in the east component of phase gradient follow previously mapped faults [green dots *Jennings* 1994] and represent small amounts of triggered slip in both right-lateral (or west-side-down) and left-lateral (or west-side-up) directions. Most of the triggered slip lies between the Landers and Hector Mine ruptures. The Emerson fault shows right-lateral triggered slip. Complex zones of surface fracturing and deformation surround the main rupture.

team of geologists [*USGS et al.*, 2000] and we use this line to define a sharp discontinuity in phase. We then extended the fault approximately 5 km on each end to account for the discontinuous phase apparent in the interferogram and counted the number of fringes between a common zero point away from the fault, and points on either side of the fault. Since the east side of the rupture moved toward the radar, the range change is mostly negative while the west side has mostly positive LOS displacement (Figure 3a). The fault forks into eastern and western branches at its southern end and we did not attempt to keep track of fringes between the strands. Over most of the fault we were able to count fringes to within 100 m of the fault trace. However, there was a segment between 12 and 20 km where counting errors are possible because the fringes were quite noisy. The total line LOS displacement (Figure 3b, dashed) has a peak value of about 2 m between 12 and 20 km from the north end of the fault; LOS displacement tapers sharply to zero to the north and more gradually to the south.

Assuming pure strike-slip motion, and accounting for the local fault orientation, one can compute the total horizontal displacement across the rupture zone; the scalebar on the right of Figure 3b is related to that total (solid). Between 22 and 30 km, the fault is almost perpendicular to the LOS vector so errors in fringe counting will be amplified by the large scale factor to convert LOS to horizontal displacement. We find horizontal offsets of 6-7 m between 12 and 28 km from the northern end of the fault. Since a small component of west-side-down offsets along the fault lowers this estimate of pure horizontal displacement, we consider this an upper bound on horizontal displacement. Upcoming ascending passes of the ERS-2 satellite will have LOS vectors that are almost parallel to the fault and thus the ascending interferograms will help to sort out the partitioning between horizontal and vertical slip.

Estimates of right-lateral, strike-slip offset made by the team geologists [*USGS et al.*, 2000] are typically 1-2 m less than our estimates. For example, they find a maximum offset of 5.2 m while we estimate offsets as high as 7 m. The distribution of offsets along the fault are in good agreement, however. The most likely explanation for the difference is that there are many very-small offset faults nearby the main rupture that cannot be detected by ground-based measurements. This difference may be resolved by more complete analysis of the InSAR data.

Triggered slip and extension

Perhaps the most important preliminary observation from the interferogram is the prevalence of triggered slip adjacent to the main rupture (Figure 4). Triggered slip occurs on the previously-mapped, parallel faults [*Jennings*, 1994] on

both sides of the main rupture and the sense of displacement switches polarity according to the lobate displacement structure of the main rupture, suggesting that this may reflect amplification of the coseismic strain change rather than a triggered response to existing tectonic stress. On the southwest side of the main rupture, the southern strands of subparallel faults (i.e., Homestead Valley, Emerson, Hidalgo, and Mesquite Lake) all display a few mm of right-lateral offset (or west-side-down). In contrast the northern strands of the connecting faults (e.g. West Calico and Rodman) display a few mm of left-lateral offset or west-side-up offset. In addition, the displacement on these faults is relatively broad compared with the right-lateral offsets to the south. Between these north and south zones lies a complex area of deformation that we interpret as extensional surface fracturing. It is interesting to note that during the Landers, 1992 rupture, the West Calico displayed right-lateral triggered slip while the slip triggered by the Hector Mine rupture on this fault is left-lateral. The north-south trending, parallel faults on the east side of the main rupture do not display triggered slip except the northern end of the Ludlow Fault (Figure 4). Finally, a broad area on the southeast side of the main rupture shows significant evidence for extensional fracturing with west side up.

Acknowledgments. We thank Howard Zebker and Evelyn Price for help in developing the InSAR processing system. Ken Hudnut provided early access to the mapping of the main rupture. Synthetic aperture radar data from the ERS-2 satellite (European Space Agency) were provided by SpotImage Co. for research use. This work was supported by NASA HPCC, JPL Contract 960884 and NSF EAR 96-19201.

References

Dibblee, T. W. Jr., Geologic map of the Lavic quadrangle, San Bernadino County, California: U.S. Geol. Survey, Misc. Geol. Investigations map, I-472, scale 1:62,500, 1966.

Dokka, R. K. and C. J. Travis, Role of the eastern California shear zone in accommodating Pacific-North American plate motion, *Geophys. Res. Lett., 17,* 1323-1327, 1990.

Goldstein, R. M., H. A. Zebker, and C. L. Werner, Satellite radar interferometry two-dimensional phase unwrapping, *Radio Sci., 23,* 713-720, 1988.

Jennings, C. W., Fault activity map of California and adjacent areas with locations And ages of recent volcanic eruptions, map scale 1:750,000, Department of Conservation, 1994.

Massonnet, D., M. Rossi, C. Carmona, F. Adragna, G. Peltzer, K. Feigl, and T. Rabaute, The displacement field of the Landers earthquake mapped by radar interferometry, *Nature, 364,* 138-142, 1993.

Massonnet, D., K. Feigl, M. Rossi and F. Adrangna, Radar interferometric mapping of deformation in the year after The Landers Earthquake, *Nature, 369,* 227-230, 1994.

Massonnet, D. and K. L. Feigl, Radar interferometry and its applicatons to changes in the Earth's surface, *Rev. Geophys., 36,* 441-500, 1998.

Michel, R. and J.-P. Avouac, Measuring near-field co-seismic displacement from SAR images: Application to the Landers Earthquake, *Geophys. Res. Lett., 26,* 3017-3020, 1999.

Peltzer, G., P. Rosen, F. Rogez and K. Hudnut, Postseismic rebound in fault step-overs caused by pore fluid, *Science, 273,* 1202-1204, 1996.

Price, E. and D. T. Sandwell, Small-scale deformations associated with the 1992 Landers, California Earthquake mapped by synthetic aperture radar interferometry phase gradients, *J. Geophys. Res., 103,* 27001-27016, 1998.

Rosen, P., S. Hensley, H. A. Zebker, F. H. Webb and E. Fielding, Surface deformation and coherence measurements of Kilauea Volcano, Hawaii from SIR-C radar interferometry, *J. Geophys. Res., 101,* 23109-23125, 1996.

Sauber, J., W. Thatcher, S. C. Solomon and M. Lisowski, Geodetic slip rate for the Eastern California Shear Zone and the recurrence time of Mojave desert earthquakes, *Nature, 367,* 264-266, 1994.

Scharroo, R., P. Visser, Precise orbit determination and gravity field improvement for the ERS satellites, *J. Geophys. Res., 103,* 8113-8127, 1998.

Stein, R. S., G. C. P. King and J. Lin, Change in failure stress on the Southern San Andreas Fault System caused by the 1992 magnitude = 7.4 Landers Earthquake, *Science, 258,* 1328-1332, 1992.

U.S. Geological Survey, the Southern California Earthquake Center, and the California Division of Mines and Geology, Preliminary Report on the 16 October 1999 M7.1 Hector Mine, California, Earthquake, *Seismol. Res. Lett.,71,* 11-23, 2000.

Zebker, H. A., P. A. Rosen, R. M. Goldstein, A. Gabriel and C. L. Werner, On the derivation of coseismic displacement fields using differential radar interferometry, *J. Geophys. Res., 99,* 19617-19643, 1994.

D. Agnew, Y. Bock, J.-B. Minster, D. Sandwell, and L. Sichoix, IGPP 0225, Scripps Institution of Oceanography, University of California, San Diego, 9500 Gilman Drive, La Jolla, CA 92093-0225. (e-mail: dagnew@ucsd.edu; ybock@ucsd.edu; jbminster@ucsd.edu; dsandwell@ucsd.edu; lydie@radar.ucsd.edu)

(Received November 5, 1999; revised March 10, 2000;
accepted May 15, 2000.)